JACS
JOURNAL OF THE AMERICAN CHEMICAL SOCIETY
Article
pubs.acs.org/JACS

Pressure-Induced Crystal Structure and Spin-State Transitions in Magnetite (Fe_3O_4)

Sheng Ju,*[,†] Tian-Yi Cai,[†] Hai-Shuang Lu,[†] and Chang-De Gong[‡,§]

[†]Department of Physics and Jiangsu Key Laboratory of Thin Films, Soochow University, Suzhou 215006, P. R. China

[‡]Center for Statistical and Theoretical Condensed Matter Physics and Department of Physics, Zhejiang Normal University, Jinhua 321004, P. R. China

[§]National Laboratory of Solid State Microstructure and Department of Physics, Nanjing University, Nanjing 210093, P. R. China

Supporting Information

ABSTRACT: High pressure is an important dimension for the emergent phenomena in transition metal oxides, including high-temperature superconductivity, colossal magnetoresistance, and magnetoelectric coupling. In these multiply correlated systems, the interplay between lattice, charge, orbital, and spin is extremely susceptible to external pressure. Magnetite (Fe_3O_4) is one of the oldest known magnetic materials and magnetic minerals, yet its high pressure behaviors are still not clear. In particular, the crystal structure of the high-pressure phase has remained contentious. Here, we investigate the pressure-induced phase transitions in Fe_3O_4 from first-principles density-functional theory. It is revealed that the net magnetic moment, arising from two ferrimagnetically coupled sublattices in Fe_3O_4, shows an abrupt drop when entering into the high-pressure phase but recovers finite value when the pressure is beyond 65.1 GPa. The origin lies in the redistribution of Fe 3d orbital occupation with the change of crystal field, where successive structural transitions from ambient pressure phase $Fd\bar{3}m$ to high pressure phase *Pbcm* (at 29.7 GPa) and further to *Bbmm* (at 65.1 GPa) are established accurately. These findings not only explain the experimental observations on the structural and magnetic properties of the highly compressed Fe_3O_4 but also suggest the existence of highly magnetized magnetite in the Earth's lower mantle.

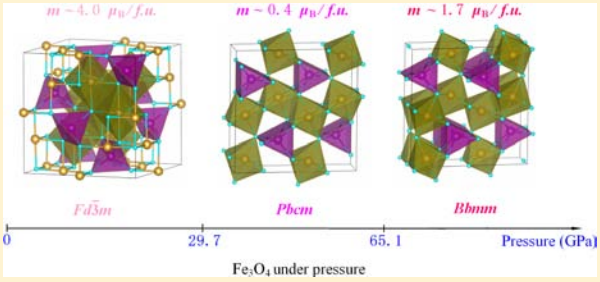

1. INTRODUCTION

Pressure-induced crystal structural transition and electronic structural transition of solids have been the focus of solid-state chemistry, material science, and condensed matter physics.[1−16] In particular, in transition metal oxides, where the interplay between lattice, spin, charge, and orbital is strong, high pressure shows significant influence on the emergent phenomena in these multiply correlated systems, including high-temperature superconductors, charge-orbital ordered manganites, Mott−Hubbard insulators, colossal magnetoresistive oxides, and magnetoelectric multiferroics.[2−16] Recently, pressure-induced simultaneous crystal structure and spin-state transitions have been found in some of 3d transition metal oxides, including $BiCoO_3$, $BiNiO_3$, $BiMnO_3$, $BiFeO_3$, $FeTiO_3$, and recently synthesized two-dimensional infinite-layer $SrFeO_2$.[5−15] High-spin-to-low-spin-state transition, accompanied by structural transition, is usually found when an external pressure is applied. For iron-related mineral oxides (FeO, Fe_2O_3, MgFeO, $MgFeSiO_3$, and $MgFeSiAlO_3$), studies on their high-pressure behaviors are meaningful not only for the fundamental research but also for the understanding of the magnetism of the Earth, where iron, as in many forms of compounds, is widely spread in the Earth's mantle.[16−28]

As one of the oldest known materials and an important constituent of the Earth's interior, magnetite (Fe_3O_4) has been the focus of high-pressure (HP) studies for many years.[29−41] At ambient conditions, Fe_3O_4 is a ferrimagnetic inverse spinel (space group $Fd\bar{3}m$, No. 227) (Figure 1a), where the tetrahedral (Td) positions are occupied by Fe^{3+} and the octahedral (Oh) sites contain equal amounts of Fe^{3+} and Fe^{2+}. Interestingly, this is the only crystal structure of Fe_3O_4 where the positions of the atoms are determined for certain. Determination of the low-temperature crystal structure is currently approached by many methods, where the Verwey transition and charge−orbital ordering are found to be intimately related with these low-temperature phases.[42−50] On the other hand, HP experimental results show that starting from 20−25 GPa (at room temperature) and up to 60 GPa, Fe_3O_4 is gradually transforming to the HP polymorph.[31−35] The exact crystal structure of the HP phase, however, is still under debate. Both $CaMn_2O_4$-type structure (space group *Pbcm*, No. 57, as shown in Figure 1b)[32] and $CaTi_2O_4$-type (space group *Bbmm*, No. 63, as shown in Figure 1c)[33−35] have been observed and proposed to be the candidate for the HP phase of Fe_3O_4. For example, as shown by Fei et al., at 34.45, 26.41, and 23.96 GPa, *Pbcm* HP phase was identified.[32] While Haavik et al. found that, from 21.8 up to 43 GPa, *Bbmm* HP

Received: May 28, 2012
Published: July 23, 2012

   dx.doi.org/10.1021/ja305167h | J. Am. Chem. Soc. 2012, 134, 13780−13786

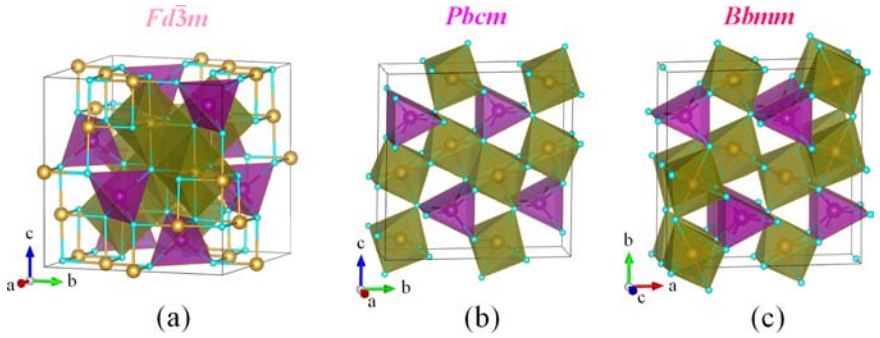

Figure 1. Illustration of crystal structure of Fe_3O_4 under ambient pressure with inverse spinel structure $Fd\bar{3}m$ (a), HP Fe_3O_4 with *Pbcm* space group (b), and HP Fe_3O_4 with *Bbmm* space group (c). Large golden balls are for Fe and small blue balls are for oxygen.

phase agrees with the elastic properties much better than *Pbcm* does.[33]

In addition, experiments on the magnetic behaviors of HP magnetite are still not clear.[36−40] A transition from the inverse spinel to the normal one was proposed first, where within a crude atomic description, a 50% change of net magnetic moment (i.e., from $S = 2$ to $S = 3$) between the inverse and normal spinel structures is expected.[37] Such an obvious variation in the magnetic moment of Fe ions, however, has not been detected by Fe K-edge X-ray magnetic circular dichroism (XMCD) measurements.[38,39] On the contrary, a sharp decrease (~50%) in the amplitude of the XMCD signal was observed between 12 and 16 GPa and was interpreted as a high-spin to intermediate-spin transition of Fe^{2+} ions at the Oh site.[38] Interestingly, in a recent XMCD experiment, neither inverse-to-normal crossover nor high-spin to intermediate-spin transition has been observed up to 41 GPa.[40] In contrast, these authors found a continuous evolution of the magnetic moment in the whole pressure range, where an abrupt drop of magnetization is revealed at around 25 GPa and the net magnetization disappears around 60−70 GPa by extrapolation to higher pressure.[40]

Hence, there has been enormous controversies on both the crystal structure and the magnetic behaviors of the compressed magnetite. In this paper, we present comprehensive first-principles studies of Fe_3O_4 under HP and provide clear answers to the following fundamental questions: What is real structure of the HP phase? Is there any intrinsic relation between the structural transitions and magnetic behaviors? If there is, what is the mechanism for the experimentally observed sharp decrease of magnetization around 25 GPa? Will the magnetization be totally lost beyond 60−70 GPa?

2. COMPUTATIONAL METHOD

Our ab initio calculations are performed using the full-potential projector augmented wave (PAW) method,[51] as implemented in the Vienna ab initio Simulation Package (VASP).[52−56] They are based on density-functional theory with the generalized gradient approximation (GGA) in the form proposed by Perdew, Burke, and Ernzerhof (PBE).[57] A large plane-wave cutoff of 1000 eV is used throughout and the convergence criteria for energy is 10^{-6} eV. PAW potentials are used to describe the electron−ion interaction with 14 valence electrons for Fe ($3p^6 3d^6 4s^2$) and 6 for O ($2s^2 2p^4$). Monkhorst−Pack *k*-point meshes are used in the Brillouin zone (BZ) integration with at least 400 *k*-points in the irreducible BZ for different crystal symmetries. In the calculations, under the certain external pressure, ions are relaxed toward equilibrium positions until the Hellman−Feynman forces are less than 1 meV/Å. The obtained lattice constant of Fe_3O_4 at ambient pressure is 8.40 Å, in good agreement with previous first-principle calculations[58] and also matching the experimental value of 8.39 Å.[58] In addition, the obtained magnetic moment is 4 μ_B/fu, agreeing with its half-metallic nature. On the other hand, we have also performed the calculations based on local spin density approximation (LSDA). However, LSDA is found to give a underestimated lattice constant of 8.09 Å as well as a low net magnetic moment of 3.28 μ_B/fu in Fe_3O_4. Compared with available experimental data of the pressure dependence of magnetization, LSDA also leads to a rapid decease of magnetization, even under low external pressures. In addition, besides the ferrimagnetic coupling between two sublattices, we also consider ferromagnetic coupled situations for both ambient pressure and HP phases. It is found that ferromagnetic ordering is energetically unfavorable. Therefore, we focus on the ferrimagnetic ordering (the ground state) in the following discussions.

3. RESULTS AND DISCUSSION

Experimentally identified $CaMn_2O_4$-type and $CaTi_2O_4$-type structures are used as starting points to search for an indeed HP phase, where the enthalpy of them are calculated as a function of external pressure together with that of $Fd\bar{3}m$ phase (Figure 2a,b). Obviously, the $Fd\bar{3}m$ phase is the ground state under ambient pressure. A transition to HP phase is found at 29.7 GPa, in agreement with the experimentally established 25 GPa.[32] Although, the enthalpy difference between *Pbcm* phase and *Bbmm* is very small, we can still see that within the range of 29.7 to 65.1 GPa, *Pbcm* is thermodynamically stable. This suggests that the first structure transition around 29.7 GPa is $Fd\bar{3}m$ to *Pbcm*, followed by the second transition from *Pbcm* to *Bbmm* at 65.1 GPa.

Examining the volume−pressure relationship (Figure 2c,d), we can further find that the relative volume change for the transition of $Fd\bar{3}m \rightarrow$ *Pbcm* is around 10.7%, which is larger than the reported experimental results, ~6.1%. The reason for this discrepancy is due to the fact that the maximum reachable pressure in the experiment is 27 GPa,[33] lower than our predicted value of 29.7 GPa. On the other hand, the transition from *Pbcm* to *Bbmm* exhibits a very small volume decrease of 0.75%. This almost negligible volume change may be responsible for the confusing experimental results of the crystal structure of HP phase.

The bulk modulus can provide additional structural information, where they are obtained by least-squares fit of the pressure−volume data to a third-order Birch−Murnaghan equation of state

$$P = \frac{3}{2}K[(V_0/V)^{7/3} - (V_0/V)^{5/3}]\left[1 - \frac{3}{4}(4 - K')\{(V_0/V)^{2/3} - 1\}\right] \quad (1)$$

dx.doi.org/10.1021/ja305167h | J. Am. Chem. Soc. 2012, 134, 13780−13786

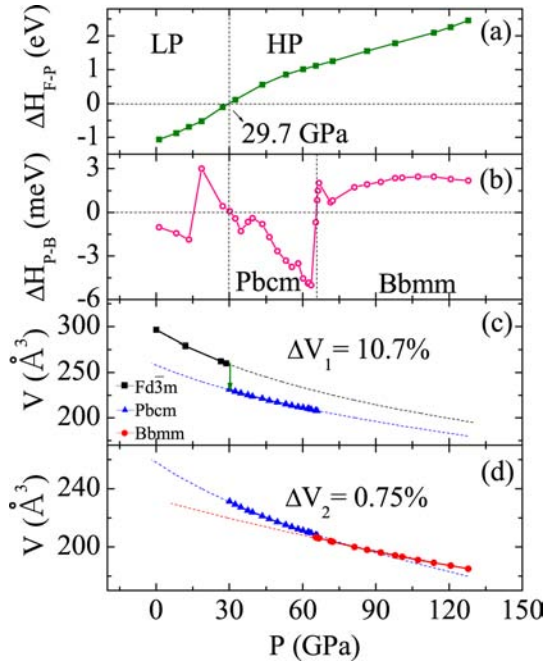

Figure 2. Thermodynamic stability diagram of Fe_3O_4 in the static approximation. (a) The enthalpy difference (per formula unit) between $Fd\bar{3}m$ and *Pbcm* phases. (b) The enthalpy difference (per formula unit) between *Pbcm* and *Bbmm* phases. (c) Pressure dependence of the volume (28-atom unit) of $Fd\bar{3}m$ and *Pbcm* phases. (d) Pressure dependence of the volume of *Pbcm* and *Bbmm* phases. The volume change at the transition pressure P_t is defined as $\Delta V = [V_1(P_t) - V_2(P_t)]/V_1(P_t)$, where 1 and 2 stand, respectively, for the phases before and after transition.

where K, K', and V_0 are the bulk modulus, its pressure derivative, and the volume at zero pressure, respectively. For $Fd\bar{3}m$ phase (P < 29.7 GPa), the bulk modulus and its pressure derivative are 181.7 ± 9.1 GPa and 2.90 ± 0.01, respectively. Within this pressure range, nine independent experimental studies as shown in Table 1 are available with bulk modulus ranging from 155 to 215 GPa,[33] in good agreement with our calculated result. For HP *Pbcm* phase (29.7 GPa < P < 65.1 GPa), a much larger bulk modulus of 234.2 ± 2.5 GPa and its pressure derivative 2.70 ± 0.09 are found, agreeing with the much denser and less compressible of HP phase. These quantities are further increased in *Bbmm* phase (65.1 GPa < P < 150 GPa), reaching 488.7 ± 7.2 GPa and 1.7 ± 0.1 for K and K', respectively. Such a large bulk modulus is consistent with 340[29] and 450 GPa[30] deduced from shock-wave experiments at pressures from 65 to 130 GPa and also verifies the fact that, between two experimentally identified HP structure candidates, *Bbmm* phase is the thermodynamically stable structure at the higher pressures. Therefore, with the above analysis and the good agreement with experimental data on elastic properties, a pressure-driven structural transition sequence of $Fd\bar{3}m$ → *Pbcm* → *Bbmm* is established.

Table 1. Calculated K (GPa) and K' in Comparison with Experimental Data as Shown in Ref 33

theory or experiment	K (GPa)	K'	P_{min}–P_{max} (GPa)
present calculations on $Fd\bar{3}m$	181.7(9.1)	2.90(0.01)	0–29.7
Bridgman (1949)	170(5)	–	0–2.9
Mao et al. (1974)	209(9)	4	0–20
Wilburn and Bassett (1977)	155(12)	4	0–6.5
Hazen et al. (1981)	189(14)	4	0–4.5
Finger et al. (1986)	186(5)	4(0.4)	0–4.5
Nakagiri et al. (1986)	181(2)	5.5(15)	0–4.5
Staun Olsen et al. (1994)	200(20)	–	0–5.5
Gerward and Staun Olsen (1995)	215(25)	7.5(40)	0–25
Haavik et al. (2000)	217(2)	4	0–27
Present calculations on HP *Pbcmm*	234.2(2.5)	2.70(0.09)	29.7–65.1
Present calculations on HP *Bbmm*	488.7(7.2)	1.70(0.10)	65.1–130.0
Ahrens et al. (1969)	340	–	65–130
Anderson and Kanamori (1968)	450	–	65–130

The evolution of magnetization of Fe_3O_4 is shown in Figure 3, where three distinct regimes compatible with the successive

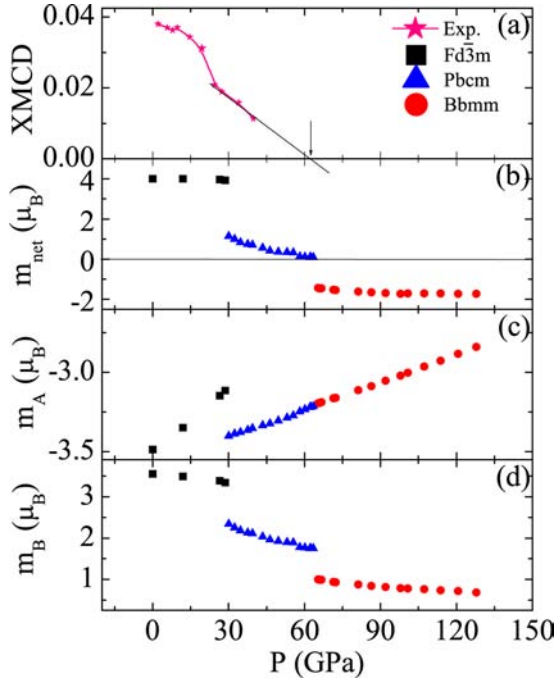

Figure 3. (a) The XMCD experimental data reproduced from ref 40. The calculated magnetic moments: (b) net moment per Fe_3O_4, (c) A site per Fe, and (d) B site per Fe.

structural transitions are obvious. The theoretically obtained net magnetic moment shows a weak pressure dependence up to 30 GPa. When entering into the *Pbcm* phase, it shows a rapid decrease at 40 GPa and total loss at 65 GPa. Furthermore, the net magnetization recovers a finite value above 65 GPa and does not disappear up to 130 GPa within *Bbmm* symmetry. It should be pointed that the revealed evolution of the magnetism is in good agreement with the XMCD experimental measurements within the range of 16–50 GPa,[40] where the observed sharp drop of magnetization can be well understood as a result of the crystal structural transition to the HP *Pbcm* phase. Within $Fd\bar{3}m$ phase or *Pbcm* phase, the experimentally measured XMCD data show a little deeper decrease than the theoretical results. This might be due to the thermal excitation effect, where the experiment was carried out at 300 K.[40] Clearly, magnetism in Fe_3O_4 is intimately related with the crystal structure. Therefore, to give a clear and comprehensive picture

dx.doi.org/10.1021/ja305167h | J. Am. Chem. Soc. 2012, 134, 13780–13786

Table 2. Space Group, Volume (28-atom unit), Energy Difference (eV/Fe) between Magnetized State and Nonmagnetized State, and Local and Net Magnetic Moments of Fe_3O_4 under Different External Pressures

sample	space group	P (GPa)	V (Å^3)	ΔE	m_A (μ_B/Fe)	m_B (μ_B/Fe)	m_{net} (μ_B/fu)
I	$Fd\bar{3}m$	0	296.5	1.0117	−3.48	3.57	4
II	$Fd\bar{3}m$	12.0	279.1	0.7925	−3.35	3.50	4
III	$Fd\bar{3}m$	28.7	260.0	0.5256	−3.11	3.36	3.93
IV	*Pbcm*	30.1	231.3	0.6240	−3.40	2.33	1.15
V	*Pbcm*	49.7	217.1	0.4928	−3.30	1.93	0.37
VI	*Pbcm*	63.4	210.1	0.4227	−3.21	1.75	0.10
VII	*Bbmm*	65.4	206.8	0.3840	−3.20	1.00	−1.33
VIII	*Bbmm*	91.9	196.1	0.3177	−3.05	0.81	−1.69
IX	*Bbmm*	100.8	193.2	0.2875	−3.00	0.78	−1.71

of pressure-induced magnetization transitions, we resort to the detailed electronic structure and spin-state at each Fe ion.

Nine representative samples as listed in Table 2 are studied in detail. The exact lattice constants and atomic positions can be found in the Supporting Information. Judging from the orbital resolved local density of states for $Fd\bar{3}m$ phase, *Pbcm* phase, and *Bbmm* phase (see Figure 4 and Supporting Information), the differences between low-pressure (LP) phases (samples I−III) and HP phases (samples IV−IX) are evident, where from orbital occupancy Fe ions are in the high-spin (HS) state for all the LP phases. For sample I, the exchange splitting energy (Δ_{EX}) between the spin-up and spin-down 3d electrons is around 3.5 eV. The crystal-field splitting energy (Δ_{CF}), i.e., the energy difference between t_{2g} and e_g states, is 0.77 eV for A site and 1.72 eV for B site (Table 3). When pressure increases to 28.7 GPa (sample III), Δ_{CF} increases to 0.92 eV for A site and 1.93 eV for B site, whereas Δ_{EX} reduces to 3.3 eV. Δ_{EX} is still larger than Δ_{CF}, leading to the HS state in all LP phases.

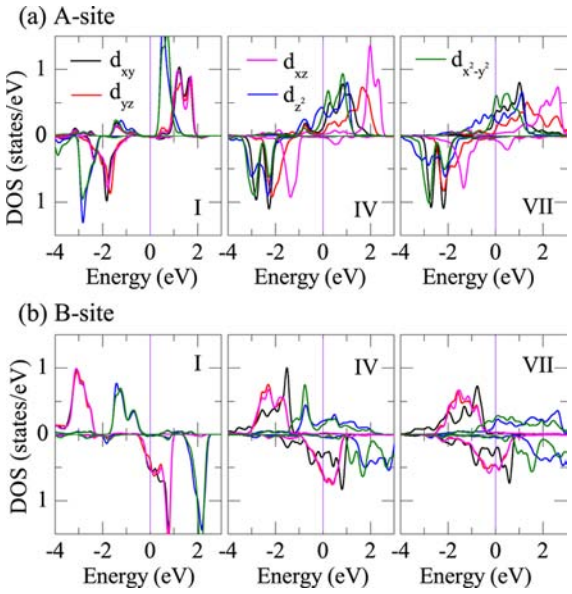

Figure 4. 3d-Orbital resolved local density of states of Fe ions: (a) A site and (b) B site. Sample I for $Fd\bar{3}m$ phase at 0 GPa, sample IV for *Pbcm* phase at 30.1 GPa, and sample VII for *Bbmm* phase at 65.4 GPa are demonstrated. The vertical line indicates the Fermi level.

On the other hand, as demonstrated in the electronic density of states (see Figure 4 and Supporting Information), Fe ions of HP phases are in the either intermediate-spin (IS) or low-spin (LS) state. For A site, the formerly empty $d^{\uparrow}_{z^2}$ orbital gets occupied, whereas $d^{\uparrow}_{yz}$ and $d^{\uparrow}_{xz}$ shift to higher energy and are still empty. Moreover, the splitting of these degenerated orbitals increases with the increasing applied pressure. Similar orbital splitting in spin-down channel is also found, where $d^{\downarrow}_{yz}$ and $d^{\downarrow}_{xz}$ states are found to move toward the Fermi level and become partially occupied with the increasing pressure. To see more clearly the pressure-induced electron redistribution among five orbitals, we demonstrate the exact orbital occupation number in Figure 5. Obviously, with the increase of pressure, electrons in the d_{yz} and d_{xz} states move to the d_{z^2} states with the opposite spin. For B site Fe, $e^{\uparrow}_g$ bands move toward the Fermi level (samples II−VI) and above the Fermi energy when the pressure is high enough (sample VII), while the states of $t^{\uparrow}_{2g}$ are still below the Fermi energy but become broadened. The expansion of $t^{\downarrow}_{2g}$ states becomes large, and $e^{\downarrow}_g$ states move to high energies. These features indicate that the electrons in the $e^{\uparrow}_g$ ($d^{\uparrow}_{z^2}$, $d^{\uparrow}_{x^2-y^2}$) states move to the $t^{\downarrow}_{2g}$ ($d^{\downarrow}_{xy}$, $d^{\downarrow}_{yz}$, and $d^{\downarrow}_{xz}$) states, as illustrated in the lower panel of Figure 5. Such a redistribution of orbital occupation reduces the spin asymmetry, leading to the IS or LS state in HP phases.

Table 3. Exchange Splitting (Δ_{EX}/eV) and Crystal Field (Δ_{CF}/eV) Deduced from Density of States for Samples I−III within $Fd\bar{3}m$ Symmetry

	Δ_{EX}		Δ_{CF}	
sample	A site	B site	A site	B site
I	3.23(0.04)	3.50(0.05)	0.77(0.02)	1.72(0.03)
II	3.22(0.04)	3.48(0.06)	0.84(0.03)	1.82(0.04)
III	3.19(0.04)	3.43(0.07)	0.92(0.04)	1.93(0.06)

In fact, the exact number of 3d electrons $n^{\uparrow}_A$ ($n^{\downarrow}_B$) increases and $n^{\downarrow}_A$ ($n^{\uparrow}_B$) decreases with the applied pressure. However, the total electron number, n_A (=$n^{\uparrow}_A$ + $n^{\downarrow}_A$) and n_B (=$n^{\uparrow}_B$ + $n^{\downarrow}_B$), remains unchanged with the increase of pressure, suggesting HP phases of Fe_3O_4 still have the chemical formula of $Fe(A)^{3+}[Fe(B)]^{2.5+}{}_2O_4$ as the magnetite at the ambient pressure. It is revealed that pressure dependence of ($n^{\uparrow}_A$ + $n^{\downarrow}_A$) and ($n^{\uparrow}_B$ + $n^{\downarrow}_B$) are almost identical with m_A and m_B demonstrated in Figure 3. This finding suggests that the evolution of magnetization can be mostly attributed to the redistribution of 3*d* orbital occupation.

Then this begs the question: why can Fe 3d orbital occupation vary with applied pressure? Our answer hinges on the nature of the crystal field, which will lead to a significant change in the environment at both A and B sites. According to Pauli's exclusion principle and Hund's rules, the spin-up and spin-down electrons will redistribute among Fe 3d orbitals, leading to the change of magnetic moment m_A and m_B. At the transition pressures, the most evident variations of crystal

dx.doi.org/10.1021/ja305167h | J. Am. Chem. Soc. 2012, 134, 13780−13786

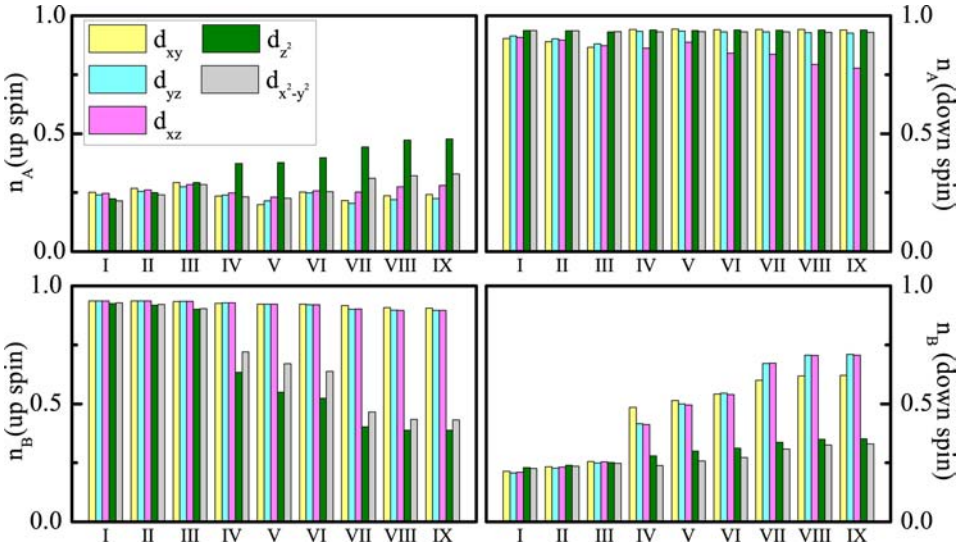

Figure 5. Orbital occupation of five 3d orbitals of Fe ions under different pressures. Both up spin and down spin channels for A site as well as B site are demonstrated.

structure occur, so the most abrupt changes of m_A and m_B are anticipated. We can take the transition $Fd\bar{3}m \rightarrow Pbcm$ as an example. The former tetrahedra becomes a trigonal prism, where two types of Fe−O bonds are involved. The former octahedra is not regular at all but heavily distorted, involving four types of Fe−O bonds. Such an obvious change of crystal field symmetry leads to the variation of 3d orbital splitting and hence the redistribution of orbital occupation. As a result, the abrupt decrease of m_A, m_B, and hence m_{net} are observed around the transition pressure (29.7 GPa). An abrupt decrease of m_B but a smooth variation of m_A can be observed around the transition pressure of $Pbcm \rightarrow Bbmm$, which can also can be understood by considering the crystal field symmetry. We calculate the length of the Fe−O bond in Figure 6. Obviously,

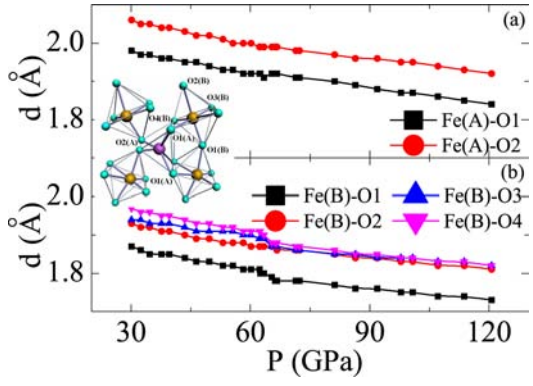

Figure 6. Pressure dependence of Fe−O bonds lengths. The inset shows the crystal structure of HP phases with trigonal prism and adjacent distorted octahedrons. Large purple and yellow spheres represent iron atoms of A and B sites, respectively, and small cyan spheres are oxygens.

the distances Fe(A)−O1 and Fe(A)−O2 decrease smoothly within the whole pressure region, indicating the trigonal prism is continuously compressed without a change of the crystal field symmetry. However, this is not the case for B site. The difference between Fe(B)−O1, Fe(B)−O3, and Fe(B)−O4 almost diminishes for *Bbmm* phase, indicating a more symmetric crystal field in *Bbmm* phase than in *Pbcm* phase. This change of crystal field symmetry leads to the discontinuity in the m_B−P curves around the transition pressure (65.1 GPa).

Finally, we summarize our revealed pressure-induced magnetic transitions in Fe_3O_4 via a spin-pairing transition picture. As shown in Figure 7, Fe^{2+} ions at B site experience two successive spin-state transitions. The number of unpaired 3d electrons decrease from five at ambient pressure to two at 29.7

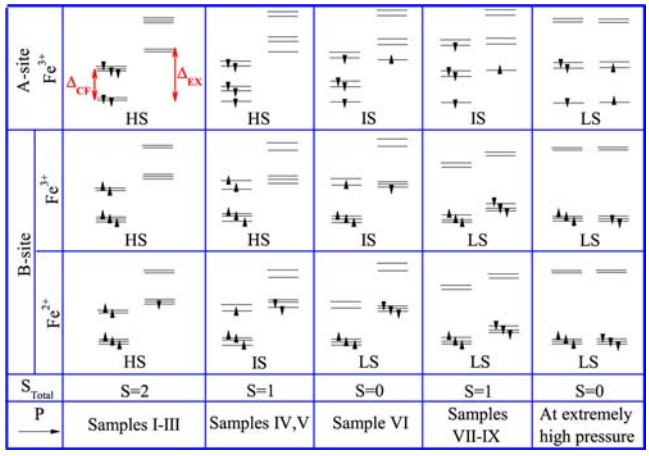

Figure 7. Spin-pairing diagram for Fe_3O_4 under external pressures. Five 3d orbitals (solid line), each capable of accommodating two electrons with opposite spins (arrows). According to the crystal field theory, in a cubic environment, the 3d orbitals split into t_{2g} and e_g levels. In a trigonal prism, the 3d orbitals split into three groups: d_{z^2}; d_{xy} and $d_{x^2-y^2}$; and d_{yz} and d_{xz}. For LP phases, since $\Delta_{EX} > \Delta_{CF}$, the first spin-down level is higher than the fifth spin-up level, with only one electron forced to pair and Fe ion has the largest number of unpaired electrons (HS state). Upon compression, crystal field splitting energy increases due to the decreasing of Fe−O bond lengths as well as degree of distortion. Given the fixed Δ_{EX}, certain lower spin-down levels will cross higher spin-up levels. When the second spin-down level crosses the fifth spin-up level, the electron at the fifth orbital will switch spin and move to the second orbital (IS state and $\Delta_{EX} \sim \Delta_{CF}$). When the third spin-down level crosses the fourth spin-up level, the electron at the fourth orbital will switch spin and move to the third orbital (LS state and $\Delta_{EX} < \Delta_{CF}$).

dx.doi.org/10.1021/ja305167h | J. Am. Chem. Soc. 2012, 134, 13780−13786

GPa, leading to the IS state. After the second structural transition, the unpaired electron number becomes zero, reaching the final LS state. Similar diagrams can be revealed for Fe^{3+} in either A or B site. Furthermore, Figure 7 shows the possible pressure-induced spin-state transition of Fe_3O_4, where Fe^{2+} in B site can have a lower spin-state transition pressure than Fe^{3+} in A and B sites, consistent with previous calculations of p−d FeO_6 cluster model.[38] As a result, pressure-induced HS−IS−LS−IS−LS transitions are observed for Fe_3O_4, which explains our calculated results of M_{net} in Figure 3b successfully. The abrupt decrease of m_{net} around 25 GPa corresponds to the HS−IS transition. The magnetic moment loss at 65 GPa is attributed to the pseudo-LS state (i.e., IS state for Fe^{3+} in A site, IS state for Fe^{3+} at B site, and LS state for Fe^{2+} at B site). Once the pressure is higher than 65 GPa, the IS−LS crossover of Fe^{3+} in B site could be the cause for the nonzero m_{net}. The true overall LS state (i.e., LS state for Fe^{2+} at B site and Fe^{3+} at A and B sites) only can be found at the highest pressure limit, where all Fe species are at LS state. On the other hand, as shown in Table 2, the energy difference between magnetized state and nonmagnetized LS state is on the order electronvolts and the value almost decreases with increasing external pressures. For sample IX at a very high pressure of around 100 GPa, the magnetized energy is 0.2875 eV, which equals to 3.333×10^3 K. Therefore, one can conclude that Fe_3O_4 could be magnetized in the Earth's lower mantle, where the pressure is around 100 GPa and the temperature is near 1000 K. Such a nonvanishing magnetic moment is important, since if the Earth's mantle contains a significant amount of magnetic minerals, it would change the way Earth's magnetic field propagates to the surface and influence the coupling between the mantle and core.

4. CONCLUSION

In conclusion, based on accurate first-principle density-functional calculations, we have studied the pressure-driven crystal structure and electronic spin-state transitions in Fe_3O_4. The crystal structure transition sequence, $Fd\bar{3}m \rightarrow Pbcm \rightarrow Bbmm$, was established accurately. Despite the negligible differences between the volume of two HP phases, the inherent bulk elastic modulus values show great differences between each other and are well described within our approach. On the other hand, the magnetization, which arises from two sublattices, shows an abrupt drop when the system transits into HP *Pbcm* phase. However, when the system further transits to HP *Bbmm* phase, the magnetization recovers the finite value. Our calculations provide a good explanation of the experimental observations of the magnetic and elastic properties in Fe_3O_4. In the meantime, the unquenched magnetic moment revealed under high pressures suggests that a highly magnetized Fe_3O_4 can exist in the Earth's lower mantle.

■ ASSOCIATED CONTENT

Supporting Information

Detailed crystal structures and electronic density of states. This material is available free of charge via the Internet at http://pubs.acs.org.

■ AUTHOR INFORMATION

Corresponding Author

jusheng@suda.edu.cn

Notes

The authors declare no competing financial interest.

■ ACKNOWLEDGMENTS

We appreciate Prof. Guang-Yu Guo, National Taiwan University, for his helpful discussions. This work was supported by the National Natural Science Foundation of China under Grants No. 10974140 and No. 11104193.

■ REFERENCES

(1) Barbee, T. W., III; Garcia, A.; Cohen, M. L. *Nature* **1989**, *340*, 369−371.
(2) Chen, X. J.; Struzhkin, V. V.; Yu, Y.; Goncharov, A. F.; Lin, C. T.; Mao, H. K.; Hemley, R. J. *Nature* **2010**, *466*, 950−953.
(3) Sun, L. L.; Chen, X. J.; Guo, J.; Gao, P.; Huang, Q. Z.; Wang, H. D.; Fang, M. H.; Chen, X. L.; Chen, G. F.; Wu, Q.; Zhang, C.; Gu, D. C.; Dong, X.; Wang, L.; Yang, K.; Li, A.; Dai, X.; Mao, H. K.; Zhao, Z. X. *Nature* **2011**, *483*, 67−69.
(4) Zhao, J.; Wang, L.; Dong, D.; Liu, Z.; Liu, H.; Chen, G.; Wu, D.; Luo, J.; Wang, N.; Yu, Y.; Jin, C.; Guo, G. *J. Am. Chem. Soc.* **2008**, *130*, 13828−13829.
(5) Oka, K.; Azuma, M.; Chen, W.; Yusa, H.; Belik, A. A.; Takayama-Muromachi, E.; Mizumaki, M.; Ishimatsu, N.; Hiraoka, N.; Tsujimoto, M.; Tucker, M. G.; Attfield, J. P.; Shimakawa, Y. *J. Am. Chem. Soc.* **2010**, *132*, 9438−9443.
(6) Azuma, M.; Carlsson, S.; Rodgers, J.; Tucker, M. G.; Tsujimoto, M.; Ishiwata, S.; Isoda, S.; Shimakawa, Y.; Takano, M.; Attfield, J. P. *J. Am. Chem. Soc.* **2007**, *129*, 14433−14436.
(7) Belik, A. A.; Yusa, H.; Hirao, N.; Ohishi, Y.; Takayama-Muromachi, E. *Chem. Mater.* **2009**, *21*, 3400−3405.
(8) Belik, A. A.; Yusa, H.; Hirao, N.; Ohishi, Y.; Takayama-Muromachi, E. *Inorg. Chem.* **2009**, *48*, 1000−1004.
(9) Ding, Y.; Haskel, D.; Tseng, Y. C.; Kaneshita, E.; van Veenendaal, M.; Mitchell, J. F.; Sinogeikin, S. V.; Prakapenka, V.; Mao, H. K. *Phys. Rev. Lett.* **2009**, *102*, 237201.
(10) Baldini, M.; Struzhkin, V. V.; Goncharov, A. F.; Postorino, P.; Mao, W. L. *Phys. Rev. Lett.* **2011**, *106*, 066402.
(11) Zhou, J. S.; Goodenough, J. B. *Phys. Rev. Lett.* **2002**, *89*, 087201.
(12) Zhou, J. S.; Alonso, J. A.; Muonz, A.; Fernandez-Diaz, M. T.; Goodenough, J. B. *Phys. Rev. Lett.* **2011**, *106*, 057201.
(13) Varga, T.; Kumar, A.; Vlahos, E.; Denev, S.; Park, M.; Hong, S.; Sanehira, T.; Wang, Y.; Fennie, C. J.; Streiffer, S. K.; Ke, X.; Schiffer, P.; Gopalan, V.; Mitchell, J. F. *Phys. Rev. Lett.* **2009**, *103*, 047601.
(14) Wu, X.; Steinle-Neumann, G.; Narygina, O.; Kantor, I.; McCammon, C.; Prakapenka, V.; Swamy, V.; Dubrovinsky, L. *Phys. Rev. Lett.* **2009**, *103*, 065503.
(15) Kawakami, T.; Tsujimoto, Y.; Kageyama, H.; Chen, X. Q.; Fu, C. L.; Tassel, C.; Kitada, A.; Suto, S.; Hirama, K.; Sekiya, Y.; Makino, Y.; Okada, T.; Yagi, T.; Hayashi, N.; Yoshimura, K.; Nasu, S.; Podloucky, R.; Takano, M. *Nat. Chem.* **2009**, *1*, 371−376.
(16) Cohen, R. E.; Mazin, I. I.; Isaak, D. G. *Science* **1997**, *275*, 654−657.
(17) Li, J.; Struzhkin, V. V.; Mao, H. K.; Shu, J.; Hemley, R. J.; Fei, Y.; Mysen, B.; Dera, P.; Prakapenka, V.; Shen, G. *Proc. Natl. Acad. Sci. U. S. A.* **2004**, *101*, 14027−14030.
(18) Speziale, S.; Milner, A.; Lee, V. E.; Clark, S. M.; Pasternak, M. P.; Jeanloz, R. *Proc. Natl. Acad. Sci. U. S. A.* **2005**, *102*, 17918−17922.
(19) Shieh, S. R.; Duffy, T. S.; Kubo, A.; Shen, G.; Prakapenka, V. B.; Sata, N.; Hirose, K.; Ohishi, Y. *Proc. Natl. Acad. Sci. U. S. A.* **2006**, *103*, 3039−3043.
(20) Shim, S. H.; Bengtson, A.; Morgan, D.; Sturhahn, W.; Catalli, K.; Zhao, J.; Lerche, M.; Prakapenka, V. *Proc. Natl. Acad. Sci. U. S. A.* **2009**, *106*, 5508−5512.
(21) Wentzcovitch, R. M.; Justo, J. F.; Wu, Z.; da Silva, C. R. S.; Yuen, D. A.; Kohlstedt, D. *Proc. Natl. Acad. Sci. U. S. A.* **2009**, *106*, 8447−8452.

(22) Miyahara, M.; Ohtani, E.; Ozawa, S.; Kimura, M.; Goresy, A.; Sakai, T.; Nagase, T.; Hiraga, K.; Hirao, N.; Ohishi, Y. *Proc. Natl. Acad. Sci. U. S. A.* **2011**, *108*, 5999−6003.
(23) Tsuchiya, T.; Wentzcovitch, R. M.; da Silva, C. R. S.; de Gironcoli, S. *Phys. Rev. Lett.* **2006**, *96*, 198501.
(24) Hsu, H.; Blha, P.; Cococcioni, M.; Wentzcovitch, R. M. *Phys. Rev. Lett.* **2011**, *106*, 118501.
(25) Saha, S.; Bengtson, A.; Crispin, K. L.; Van Orman, J. A.; Morgan, D. *Phys. Rev. B* **2011**, *84*, 184102.
(26) Hirose, K. *Science* **2010**, *327*, 151−152.
(27) Irifune, T.; Shinmei, T.; McCammon, C. A.; Miyajima, N.; Rubie, D. C.; Frost, D. J. *Science* **2010**, *327*, 193−195.
(28) Bovlol, C. I. *Phil. Trans. R. Soc. A* **2005**, *363*, 2811−2836.
(29) Ahrens, T. J.; Anderson, D. J.; Ringwood, A. E. *Rev. Geophys.* **1969**, *7*, 667.
(30) Anderson, D. L.; Kanamori, H. *J. Geophys. Res.* **1968**, *73*, 6477.
(31) Hwang, E.; Bassett, W. A. *J. Geophys. Res.* **1986**, *91*, 4697−4703.
(32) Fei, Y. W.; Frost, F. J.; Mao, H. K.; Prewitt, C. T.; Hausermann, D. *Am. Mineral.* **1999**, *84*, 203−206.
(33) Haavik, C.; Stolen, S.; Fjellvag, H.; Hanfland, M.; Hausermann, D. *Am. Mineral.* **2000**, *85*, 514−523.
(34) Dubrovinsky, L. S.; Dubrovinskaia, N. A.; McCammon, C.; Rozenberg, G. K.; Ahuja, R.; Osorio-Guillen, J. M.; Dmitriev, V.; Weber, H. P.; Bihan, T. L.; Johansson, B. *J. Phys.: Condens. Matter* **2003**, *15*, 7697−7706.
(35) Lazor, P.; Shebanova, O. N.; Annersten, H. *J. Geophys. Res.* **2004**, *109*, B05201.
(36) Xu, W. M.; Machavariani, G. Y.; Rozenberg, G. K.; Pasternak, M. P. *Phys. Rev. B* **2004**, *70*, 174106.
(37) Rozenberg, G. K.; Amiel, Y.; Xu, W. M.; Pasternak, M. P.; Jeanloz, R.; Hanfland, M.; Taylor, R. D. *Phys. Rev. B* **2007**, *75*, 020102.
(38) Ding, Y.; Haskel, D.; Ovchinnikov, S. G.; Tseng, Y. C.; Orlov, Y. S.; Lang, J. C.; Mao, H. K. *Phys. Rev. Lett.* **2008**, *100*, 045508.
(39) Subias, G.; Cuartero, V.; Garcia, J.; Blasco, J.; Mathon, O.; Pascarelli, S. *J. Phys.: Conf. Ser.* **2009**, *190*, 012089.
(40) Baudelet, F.; Pascarelli, S.; Mathon, O.; Itie, J. P.; Polian, A.; Chervin, J. C. *Phys. Rev. B* **2010**, *82*, 140412(R).
(41) Glazyrin, K.; McCammon, C.; Dubrovinsky, L.; Merlini, M.; Schollenbruch, K.; Woodland, A.; Hanfland, M. *Am. Mineral.* **2012**, *97*, 128−133.
(42) Verwey, E. J. W. *Nature* **1939**, *144*, 327−328.
(43) Senn, M. S.; Wright, J. P.; Attfield, J. P. *Nature* **2012**, *481*, 173−176.
(44) Wright, J. P.; Attfield, J. P.; Radaelli, P. G. *Phys. Rev. Lett.* **2001**, *87*, 266401.
(45) Blasco, J.; Garcia, J.; Subias, G. *Phys. Rev. B* **2011**, *83*, 104105.
(46) Leonov, I.; Yaresko, A. N.; Antonov, V. N.; Korotin, M. A.; Anisimov, V. I. *Phys. Rev. Lett.* **2004**, *93*, 146404.
(47) Jeng, H. T.; Guo, G. Y.; Huang, D. J. *Phys. Rev. Lett.* **2004**, *93*, 156403.
(48) Jeng, H. T.; Guo, G. Y.; Huang, D. J. *Phys. Rev. B* **2006**, *74*, 195115.
(49) Rozenberg, G. Kh.; Pasternak, M. P.; Xu, W. M.; Amiel, Y.; Hanfland, M.; Amboage, M.; Taylor, R. D.; Jeanloz, R. *Phys. Rev. Lett.* **2006**, *96*, 045705.
(50) Piekarz, P.; Parlinski, K.; Oles, A. M. *Phys. Rev. Lett.* **2006**, *97*, 156402.
(51) Blochl, P. E. *Phys. Rev. B* **1994**, *50*, 17953.
(52) Kresse, G.; Furthmuller, J. *Comput. Mater. Sci.* **1996**, *6*, 15.
(53) Blochl, P. E.; Jepsen, O.; Andersen, O. K. *Phys. Rev. B* **1994**, *49*, 16223.
(54) Kresse, G.; Hafner, J. *Phys. Rev. B* **1993**, *47*, 558.
(55) Kresse, G.; Hafner, J. *Phys. Rev. B* **1994**, *49*, 14251.
(56) Kresse, G.; Joubert, D. *Phys. Rev. B* **1999**, *59*, 1758.
(57) Perdew, J. P.; Burke, K.; Ernzerhof, M. *Phys. Rev. Lett.* **1996**, *77*, 3865.
(58) Friak, M.; Schindlmayr, A.; Scheffler, M. *New J. Phys.* **2007**, *9*, 5.